

# Global Biogeochemical Cycles®

## RESEARCH ARTICLE

10.1029/2021GB007146

### Key Points:

- Waterbody size and shape have strong nonlinear effects on CO<sub>2</sub>, with the highest concentrations in small, complex, waterbodies
- Dissolved organic carbon quantity and composition are the most important drivers of CH<sub>4</sub> concentrations in waterbodies
- Wildfires increase the sensitivity of waterbody CO<sub>2</sub> and CH<sub>4</sub> concentrations to degraded permafrost in upstream watersheds

### Supporting Information:

Supporting Information may be found in the online version of this article.

### Correspondence to:

S. M. Ludwig,  
sml2278@columbia.edu

### Citation:

Ludwig, S. M., Natali, S. M., Mann, P. J., Schade, J. D., Holmes, R. M., Powell, M., et al. (2022). Using machine learning to predict inland aquatic CO<sub>2</sub> and CH<sub>4</sub> concentrations and the effects of wildfires in the Yukon-Kuskokwim Delta, Alaska. *Global Biogeochemical Cycles*, 36, e2021GB007146. <https://doi.org/10.1029/2021GB007146>

Received 10 AUG 2021  
Accepted 16 MAR 2022

## Using Machine Learning to Predict Inland Aquatic CO<sub>2</sub> and CH<sub>4</sub> Concentrations and the Effects of Wildfires in the Yukon-Kuskokwim Delta, Alaska

Sarah M. Ludwig<sup>1</sup> , Susan M. Natali<sup>2</sup>, Paul J. Mann<sup>3</sup> , John D. Schade<sup>2</sup>, Robert M. Holmes<sup>2</sup>, Margaret Powell<sup>4</sup>, Greg Fiske<sup>2</sup>, and Roisin Commane<sup>1</sup> 

<sup>1</sup>Department of Earth and Environmental Science, Columbia University, New York, NY, USA, <sup>2</sup>Woodwell Climate Research Center, Falmouth, MA, USA, <sup>3</sup>Department of Geography and Environmental Science, Northumbria University, Newcastle Upon Tyne, UK, <sup>4</sup>Department of Earth and Planetary Sciences, Harvard College, Cambridge, MA, USA

**Abstract** Climate change is causing an intensification in tundra fires across the Arctic, including the unprecedented 2015 fires in the Yukon-Kuskokwim (YK) Delta. The YK Delta contains extensive surface waters (~33% cover) and significant quantities of organic carbon, much of which is stored in vulnerable permafrost. Inland aquatic ecosystems act as hot-spots for landscape CO<sub>2</sub> and CH<sub>4</sub> emissions and likely represent a significant component of the Arctic carbon balance, yet aquatic fluxes of CO<sub>2</sub> and CH<sub>4</sub> are also some of the most uncertain. We measured dissolved CH<sub>4</sub> and CO<sub>2</sub> concentrations ( $n = 364$ ), in surface waters from different types of waterbodies during summers from 2016 to 2019. We used Sentinel-2 multispectral imagery to classify landcover types and area burned in contributing watersheds. We develop a model using machine learning to assess how waterbody properties (size, shape, and landscape properties), environmental conditions (O<sub>2</sub>, temperature), and surface water chemistry (dissolved organic carbon composition, nutrient concentrations) help predict in situ observations of CH<sub>4</sub> and CO<sub>2</sub> concentrations across deltaic waterbodies. CO<sub>2</sub> concentrations were negatively related to waterbody size and positively related to waterbody edge effects. CH<sub>4</sub> concentrations were primarily related to organic matter quantity and composition. Waterbodies in burned watersheds appeared to be less carbon limited and had longer soil water residence times than in unburned watersheds. Our results illustrate the importance of small lakes for regional carbon emissions and demonstrate the need for a mechanistic understanding of the drivers of greenhouse gases in small waterbodies.

## 1. Introduction

The Arctic stores vast quantities of carbon in soil and permafrost, perennially frozen ground, that is sequestered from the active carbon cycle. Approximately twice as much carbon is stored in permafrost globally as is currently in the entire atmosphere (Hugelius et al., 2014, 2020). The Arctic is now warming at an accelerated rate and recent research has shown that increasing emissions of CH<sub>4</sub> and CO<sub>2</sub> from ecosystems is causing the Arctic to switch from a net sink to a net source of carbon to the atmosphere in some locations (Belshe et al., 2013; Schuur et al., 2015; Virkkala et al., 2021; Watts et al., 2021). As permafrost thaws, modern soil and permafrost-derived carbon is then decomposed by soil microorganisms and respired as carbon dioxide (CO<sub>2</sub>) or methane (CH<sub>4</sub>), which are either emitted to the atmosphere directly, or transported through landscapes via ground and surface waters to inland waterbodies (Schuur et al., 2008, 2015). Globally, inland aquatic waterbodies receive approximately 2–3 Pg-C yr<sup>-1</sup> from terrestrial landscapes, of which 0.8–2.1 Pg-C yr<sup>-1</sup> is thought to be processed and emitted to the atmosphere as CO<sub>2</sub> (Cole et al., 2007; Raymond et al., 2013; Tranvik et al., 2009). This makes inland aquatic CO<sub>2</sub> emissions comparable to those estimated from global land use change (IPCC, 2013). Inland aquatic waterbodies can also act as globally significant sources of CH<sub>4</sub> to the atmosphere. CH<sub>4</sub> has 25-times the global warming potential of CO<sub>2</sub> over a 100-year time period (Boucher et al., 2009). Methane emissions from inland waters are estimated at 0.65 Pg of C yr<sup>-1</sup> (CO<sub>2</sub>-eq), which is 25% of the global estimated land greenhouse gas sink (Bastviken et al., 2011). Despite the potentially pivotal role of inland aquatic ecosystems in the global carbon budgets, the uncertainty in inland aquatic fluxes is of the same magnitude as the fluxes themselves (Raymond et al., 2013; Regnier et al., 2013).

In high-latitudes, the inland water carbon emissions are particularly important because lateral carbon transport plays an outsized role in terrestrial carbon cycling (Chapin & Woodwell, 2006; Tranvik et al., 2009). As much as twenty-percent of terrestrial net ecosystem productivity is transferred to aquatic environments as dissolved

inorganic carbon (Kling et al., 1991; Stackpole et al., 2017). The distribution of waterbodies in high-latitudes is dominated by small waterbodies ( $<0.001 \text{ km}^2$ ), which are the highest potential emitters of  $\text{CO}_2$  and  $\text{CH}_4$  to the atmosphere. These small water bodies are also the most difficult to accurately map, and, therefore, they are often not considered in “bottom-up” scaling estimates (Holgerson & Raymond, 2016; Hotchkiss et al., 2015; Muster et al., 2019; Thornton et al., 2016). One exception, a recent bottom-up meta-analysis found aquatic emissions contribute up to 50% of global methane emissions (Rosentreter et al., 2021). In this study, lakes were the second largest contributor behind freshwater wetlands, with approximately 50% of lake emissions coming from the smallest waterbodies ( $<0.001 \text{ km}^2$ ) and 62% of lake emissions coming from those under  $0.01 \text{ km}^2$ . It is critical to reduce uncertainty in inland aquatic carbon fluxes and predict whether carbon is emitted as  $\text{CH}_4$  or  $\text{CO}_2$  to understand feedbacks to climate.

Wildfire frequency and severity are also increasing in high latitudes, with both direct (i.e.,  $\text{CH}_4$  and  $\text{CO}_2$  emissions from combustion) and indirect (e.g., decreases in soil respiration but an increase in permafrost thaw) feedbacks to climate (Boby et al., 2010; Bond-Lamberty et al., 2007, 2004; Kasischke et al., 2010; Mack et al., 2008). Wildfires and permafrost thaw can affect landscape-level carbon dynamics in the Arctic through changing vegetation, energy balance, soil respiration, and hydrology (Alexander et al., 2018; Dooley & Treseder, 2011; Helbig et al., 2016; Jiang et al., 2017). Landscape-level processes can have consequences for waterbodies through influence over lateral transport, in turn regulating the quality and quantity of dissolved carbon and the availability of limiting nutrients as well as environmental conditions such as water temperature, oxygen content, and pH (Abbott et al., 2021; Hutchins et al., 2020; Vonk et al., 2015). Wildfires and permafrost thaw also affect the extent and distribution of waterbodies through both the formation of new waterbodies from permafrost subsidence and the draining of existing waterbodies from deepening thaw (Brown et al., 2015; Jorgenson et al., 2010; Jorgenson & Osterkamp, 2005; Minsley et al., 2016; Walvoord & Kurylyk, 2016).

Aquatic carbon dynamics are regulated at a hierarchy of scales, ranging from regional climate and substrate characteristics, to watershed-level vegetation, landscape connectivity, and disturbance, and internal processes (Lapierre & del Giorgio, 2012; Toming et al., 2020). The complex mechanisms that influence dissolved  $\text{CO}_2$  and  $\text{CH}_4$  in waterbodies make modeling inland aquatic carbon fluxes difficult, regardless of the type of model used. This complexity is a large reason for the uncertainty in inland aquatic carbon emissions, as many estimates are based on scaling average fluxes by lake size or simple linear regression models with one or two drivers that leave large amounts of variance unexplained. Interpreting the role of wildfire can be particularly challenging, as the effects of wildfires interact with nonlinear mechanisms operating at multiple scales (Hutchins et al., 2020).

The Yukon-Kuskokwim (YK) Delta is an ideal ecosystem to study the hierarchical mechanisms driving carbon cycling in permafrost landscapes. The YK Delta, the largest wetland on the west coast of North America ( $\sim 1 \times 10^5 \text{ km}^2$ ), is subarctic tundra underlain by discontinuous permafrost, but near surface permafrost temperatures are near the point of thaw ( $\sim 1 \text{ m}$  depth; S.M. Natali, unpublished data). YK Delta is subject to frequent wildfires, but more area burned in the YK Delta in 2015 than in the previous five decades combined (BLM-AICC Alaska Wildland Fire Maps). Atmospheric inverse models of the circumpolar Arctic and high latitudes using airborne  $\text{CO}_2$  and  $\text{CH}_4$  data have shown the YK Delta to be a regional hotspot of  $\text{CO}_2$  and  $\text{CH}_4$  emissions (Chang et al., 2014; Chen et al., 2015; Commane et al., 2017; Miller et al., 2016), but there have been few on the ground measurements of fluxes to properly identify and attribute the specific ecosystems and mechanisms contributing to these fluxes (Bartlett et al., 1992; Fan et al., 1992).

In order to evaluate the relationship between wildfires and inland aquatic carbon in the YK Delta, we require an approach that can accommodate the complex effects of fire and the potentially hierarchical and nonlinear functional relationships. In this study, we used boosted regression tree models to investigate environmental variables influencing dissolved  $\text{CO}_2$  and  $\text{CH}_4$  in surface waters from wetlands and small waterbodies in the YK Delta in Alaska. We evaluated the effect of fire on drivers of  $\text{CO}_2$  and  $\text{CH}_4$  in waterbodies by training separate boosted regression tree models for burned and unburned watersheds. We used the relative influence of a suite of drivers to rank which variable can best explain the variability in  $\text{CO}_2$  and  $\text{CH}_4$ , including environmental variables (e.g., dissolved oxygen, temperature, pH), waterbody size and shape, watershed landscape characteristics (e.g., average slope, percent cover burned area), and waterbody chemistry (e.g., dissolved organic carbon (DOC) concentration and composition,  $\text{NH}_4^+$ ,  $\text{NO}_3^-$ ,  $\text{PO}_4^{3-}$ ). We described the relationship between the most important drivers and dissolved  $\text{CO}_2$  and  $\text{CH}_4$  to (a) examine implications for process-based models and scaling waterbody  $\text{CO}_2$  and

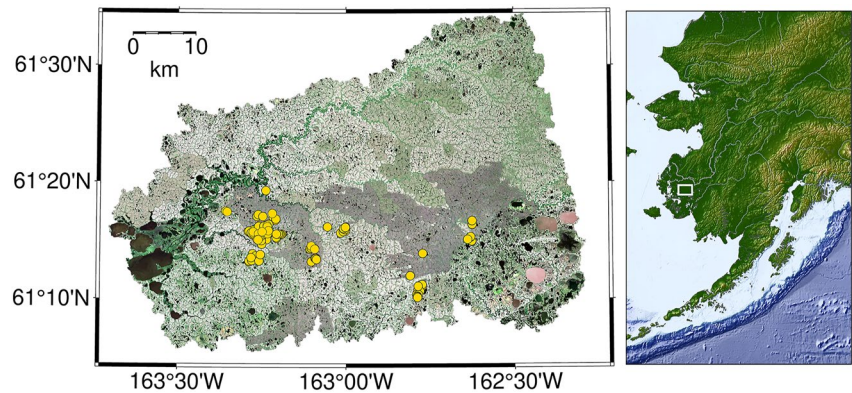


**Figure 1.** Yukon Kuskokwim Delta of Alaska (left), study region (inset). Sentinel-2 10 m resolution RGB imagery of the study region (right). Surface water sample locations from 2016 to 2019 are depicted as yellow points.

$\text{CH}_4$ , and (b) examine how the processes controlling  $\text{CO}_2$  and  $\text{CH}_4$  relationships between landscapes and aquatic ecosystems may be altered under a warming climate (e.g., increased wildfire).

## 2. Materials and Methods

### 2.1. Site Description

This study was conducted in the central-interior of the YK Delta of Alaska, a subarctic tundra region underlain by discontinuous permafrost (Figure 1). The study region was located near the Kuka Creek fires of 2015 (N 61.26°, W 163.25°), about 90 km NW of Bethel, AK, and about 110 km inland from the coast. Average air temperatures in Bethel, AK are  $-0.4^\circ\text{C}$  annually,  $12.4^\circ\text{C}$  in summer (June, July and August),  $-12.2^\circ\text{C}$  in winter (December, January, and February), and above freezing from May–October (National Weather Service; Bethel area, 1981–2020). Average annual precipitation is 480 mm, with 188 mm falling in summer on average. Thaw depths were 30–40 cm in June and July 2016–2017, and 60–70 cm in September 2016. Organic layer horizons were deep, ranging from 30–75 cm at the surface. Lakes cover approximately one third of the region and range in area from several  $\text{m}^2$  to several  $\text{km}^2$ . Lake depths were typically uniformly shallow ( $<2$  m) and well-mixed. The remaining landscape is a patchwork of raised peat plateaus and low-lying wetlands, with elevation varying from 11–35 m above sea level. Vegetation on the peat plateaus can be characterized as dwarf shrub lichen tundra, with various lichen species and *Sphagnum fuscum* dominant by biomass. Other common plants include *Betula nana*, *Empetrum nigrum*, *Oxycoccus microcarpus*, *Rhododendron subarcticum*, *Rubus chamaemorus*, *Vaccinium uliginosum*, *Vaccinium vitis-idaea*, and graminoids including *Eriophorum angustifolium*, and *Eriophorum vaginatum*.

### 2.2. Sample Collection and Processing

#### 2.2.1. Water Sample Collection

Surface water samples ( $n = 364$ ) were collected across 4 years of field campaigns (2016–2019). Of these surface water samples,  $n = 294$  were analyzed for dissolved  $\text{CH}_4$  and  $n = 235$  for dissolved  $\text{CO}_2$  from 201 distinct waterbodies. Several waterbodies were sampled in multiple years and the largest water bodies were sampled in multiple locations. Approximately 45% of the waterbodies sampled were lakes, 40% of the waterbodies sampled were fen surface waters, and the remainder of the waterbodies sampled were streams, small ponds, and surface waters on peat plateaus. While there are some clear differences between lakes, streams, and fens for example, many waterbodies exist on a continuum between such designations and these categories do not capture that complexity. Samples were collected between mid-June and mid-July. Surface water samples were immediately filtered through pre-combusted GF/F filters (Whatman nominal pore-size  $\sim 0.7 \mu\text{m}$ ), portioned into sample-rinsed 20-ml polycarbonate containers, stored in the dark at  $\sim 4^\circ\text{C}$ , and frozen within 48 hr until subsequent analyses.

### 2.2.2. Dissolved Gas Collection and Analysis

For each sample observation, three dissolved gas measurements were collected simultaneously and processed individually, with their average reported as the observation. Dissolved gases were collected by a headspace-equilibration method. For each triplicate, 30 ml of bubble-free surface water was slowly drawn into a syringe. Next 30 ml of ambient air was drawn and the syringe sealed. Each syringe was vigorously shaken for exactly 1 min while maintained at the temperature of the waterbody sampled. After equilibration, the headspace was injected into evacuated, double septum, vials until slightly over-pressurized. The gas vials were shipped to Woodwell Climate Research Center and analyzed for CH<sub>4</sub> and CO<sub>2</sub> concentrations using a Shimadzu GC-2014 gas chromatograph within several weeks of collection. Additional gas vials were injected in the field with ambient air to correct for the introduced headspace concentrations. Additional gas vials were injected in the field with standard gasses, and the accurate recovery of these concentrations was used to verify the integrity of gas vials during transportation. Dissolved gas concentrations were corrected for solubility using the water temperature and air pressure at the time of equilibration. Surface water temperature, pressure, dissolved oxygen (% and mg/L), and pH were measured using a YSI Pro-Plus multiparameter instrument. The YSI probes were calibrated daily using NIST standards (pH 4 and 7). Dissolved CH<sub>4</sub> gas samples were analyzed for stable carbon isotopic composition at Northumbria University using a Delta V Plus IRMS interfaced to a Trace Gas Pre-Concentrator and Gas Bench (Thermo Scientific). Dissolved CH<sub>4</sub> isotopic signatures were corrected for atmospheric mixing during headspace equilibration assuming global mean surface atmospheric  $\delta^{13}\text{C-CH}_4$  of  $-47.2\text{‰}$  (Warwick et al., 2016).

### 2.2.3. Water Sample Chemistry

Surface water samples were analyzed for DOC and total dissolved nitrogen concentrations using a Shimadzu TOC-VCPH at the Woodwell Climate Research Center. Nutrient concentrations, including phosphate, nitrate, and ammonium, were analyzed colorimetrically on an Astoria-Pacific autoanalyzer at the Woodwell Climate Research Center. Nitrate concentrations were often below levels of detection, and henceforth we report dissolved inorganic nitrogen as the sum of ammonium and nitrate concentrations. Chromophoric dissolved organic matter (DOM) was measured on surface water samples using a Shimadzu UV-Vis spectrophotometer measuring absorbance across 200–800 nm wavelengths at 1 nm resolution. Specific UV absorbance at 254 nm (SUVA) and the DOM slope ratio ( $S_R$ ) were then calculated as in Helms et al. (2008) as indicators of carbon composition and lability. The slope ratio of DOM is inversely related to the average molecular weight of DOM; a higher slope ratio indicates lower bulk molecular weight, which is commonly a more labile carbon source for decomposition (Helms et al., 2008). SUVA is directly related to average DOM aromaticity, which usually corresponds to higher contributions of biologically unreactive carbon sources (Helms et al., 2008).

## 2.3. Geospatial Waterbody and Watershed Analyses

We used remote sensing to quantify watershed characteristics that might be related to unmeasured landscape variables (e.g., watershed thaw depth), hydrologic variables (e.g., water residence time) and unmeasured reactants (e.g., black carbon, organic-phosphorus). Map figures were created using Generic Mapping Tools (Wessel et al., 2019).

### 2.3.1. Watershed Imagery Processing

To evaluate the role of watershed inputs and landscape connectivity on dissolved CO<sub>2</sub> and CH<sub>4</sub> concentrations, we delineated watersheds for each sampling location using the SAGA “Upslope area” algorithm in QGIS with a 2-m resolution digital elevation model (Porter et al., 2018). Level-2A Sentinel-2, 10-m resolution, multispectral surface reflectance imagery was used to provide information on vegetation, landcover, and surface water. The surface reflectance imagery was a composite of cloud-free imagery from 2017 to 2019 within 2 weeks of most sample collection dates (early July). The surface reflectance imagery was used to calculate the Normalized Difference Water Index (NDWI) and Normalized Difference Vegetation Index (NDVI), metrics of canopy or soil moisture and vegetation productivity. We calculated slope and elevation from the digital elevation model. We then determined the average of each derived index by sample watershed to include as potential drivers in modeling dissolved CO<sub>2</sub> and CH<sub>4</sub>. The composite imagery and derived indices were made using Google Earth Engine.

**Table 1**  
*Boosted Regression Tree Model Fit and Predictive Ability*

Model	Number of variables	Number of observations	$R^2$	Variance predicted (%)	RMSE (log $\mu\text{M}$ )
CO <sub>2</sub> Unburned	13	93	0.94	79%	0.55
CO <sub>2</sub> Burned	15	142	0.87	61%	0.73
CH <sub>4</sub> Unburned	17	121	0.88	52%	0.28
CH <sub>4</sub> Burned	18	166	0.79	36%	0.47

*Note.* Coefficient of determination ( $R^2$ ) from a linear regression of modeled and observed log concentrations. Variance explained (%) and root mean square error (RMSE) from predictive deviance of 10-fold cross validations.

### 2.3.2. Landcover Mapping

We created a 10-m resolution landcover map for the region of interest to determine the presence and abundance of various terrestrial, wetland, surface waterbodies, and disturbed areas in sample watersheds (Figure S1 in Supporting Information S1). We used an unsupervised k-means algorithm (Google Earth Engine, “wekaKMeans”) with the surface reflectance raw bands, derived bands (NDWI, NDVI), slope, and elevation as inputs for the classification. The Alaska Interagency Coordination Center historical wildfire database was used for wildfire delineations. Wildfires in the region of interest included fire scars from the 1970s, 1990s, and early 2000s, collectively designated as “old fires,” and fire scars from the large area burned in 2015. First, the region of interest was divided into unburned, old fire scars, and 2015 fire scars, and the classification algorithm was run separately for each. We used an initial number of classes “k” higher than the number of known landcover types in order to capture the variability in the driving layers,

then later grouped similar classes produced by the k-means algorithm. For example, the unburned classification identified three classes grouped as terrestrial peat plateau tundra and two wetland classes merged as peatland fens. The final landcover classes for unburned areas include terrestrial peat plateau, peat plateau edges, degraded peat plateau (i.e., from permafrost thaw), fens, and surface water. The final landcover classes for old fire scars and 2015 fire scars include peat plateau, degraded peat plateau, fens, and surface water. We calculated the total area and percent area of each landcover type and burned area by sample watershed to include as potential drivers in modeling dissolved CO<sub>2</sub> and CH<sub>4</sub>. Landcover accuracy was assessed using 350 randomly stratified points from the region of interest. The classifications at these points were compared to higher resolution (Worldview-2) imagery using Google Earth Engine and reclassified using expert assessment. We used a confusion matrix to assess the balanced accuracy of each classification, which ranged from 0.75 to 0.99 (Figure S2 in Supporting Information S1) (Clewley et al., 2015).

### 2.3.3. Waterbody Shape

To determine the effects of waterbody shape on dissolved CO<sub>2</sub> and CH<sub>4</sub>, we calculated the area and perimeter of every surface waterbody in the region of interest using object-based image analysis in Google Earth Engine. Each sample location with a large enough waterbody to be detected was then assigned the corresponding area, perimeter, and area:perimeter ratio. The waterbody shape data were mostly only available for sample locations classified as lakes, as the amount of surface water in fens, streams, and plateau ponds was often too small to detect at 10 m resolution.

## 2.4. Statistical Analysis

We used boosted regression tree models to predict dissolved CO<sub>2</sub> and CH<sub>4</sub> and explore the effect of fire on the relationships between potential drivers and CO<sub>2</sub> and CH<sub>4</sub>. Boosted regression tree (also called gradient boosting) is a form of machine learning developed from the decision tree family of models combined with a boosting algorithm. Recent studies have used machine learning approaches to create statistical models with greater accuracy in predicting ocean surface dissolved CO<sub>2</sub> and DOC in inland waterbodies (Chen et al., 2019; Toming et al., 2020). These models have higher accuracy because they allow for complex interactions and non-linear relationships, which often better capture the mechanisms involved. All boosted regression tree models were fit using the “gbm” function in the gbm package in R v.3.6.1, and model results were investigated using the “ice” function in the ICEbox package in R v.3.6.1. Model fit was investigated by linear regression (“lm” function in R) between observed dissolved gas concentrations and the predicted dissolved gas concentrations from the boosted regression tree model results. Both dissolved CO<sub>2</sub> and CH<sub>4</sub> concentrations were log-transformed to achieve normality which was assessed using QQ-norm plots (“qqnorm” function in R).

### 2.4.1. Driver Selection and Model Structure

In order to capture potentially disparate effects of fire on the drivers of dissolved CO<sub>2</sub> and CH<sub>4</sub>, we split the data set into observations with mostly unburned watersheds (<10% burn area) and burned watersheds (>10% burn area) and modeled them separately (Table 1). The majority of watersheds affected by fire were only partially

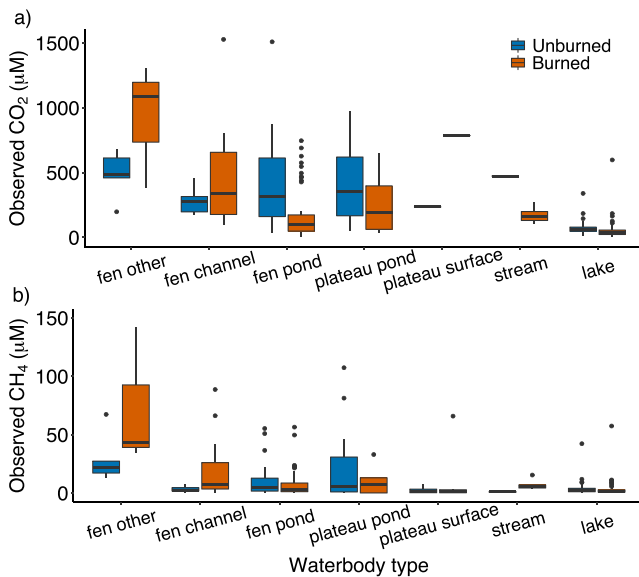


**Figure 2.** Observed dissolved gas concentrations for CO<sub>2</sub> (a) and CH<sub>4</sub> (b) by waterbody type and separated into unburned (blue) and burned (orange) watersheds. The lower and upper hinges correspond to the first and third quartiles, the whiskers extend to 1.5 times the interquartile range, with outliers indicated as points.

burned and few watersheds were completely within the 2015 Kuka Creek fire scar. Varying the cutoff from >0% watershed area burned through 33% area burned had little effect on model fitting or results. Dissolved CO<sub>2</sub> and CH<sub>4</sub> were log transformed to achieve normality. Several possible variables were excluded from the model due to strong correlations (Pearson correlation >0.7) with other drivers. While boosted regression tree models can accommodate correlated predictor variables, interpretations of variable importance are difficult in such circumstances. For example, watershed average NDWI and NDVI correlate strongly, so we chose to retain NDWI as it can also serve as a proxy for soil moisture which has direct consequences for CO<sub>2</sub> and CH<sub>4</sub> production. Dissolved organic nitrogen concentration was excluded due to the high correlation with DOC concentration. The classified percent area of landcover types in the watersheds necessarily sum to one and are therefore often highly correlated. We included only the landcover types that are expected to be more ecologically important.

#### 2.4.2. Model Training

Boosted regression tree model training was performed using the “gbm.step” function from the *dismo* package in R v.3.6.1 following the procedure in Elith et al. (2008). We used a learning rate and bag fraction of 0.005 and 0.65 respectively, which are within the optimum ranges. Changes in the learning rate and bag fraction had little effect on model performance. We used a tree complexity of 2, allowing for two-way interactions between predictors. Small sample sizes for boosted regression tree models, such as the data set in this study, are generally best modeled with tree complexity two or three and ≥1,000 trees. We saw no substantial difference in the model when increasing tree complexity to 3. We used 10-fold cross-validation to tune the number of trees and drop variables to avoid over-fitting. We used deviance as a loss function, a goodness-of-fit metric (*D*) related to the difference in log-likelihoods of the fitted model (*L<sub>m</sub>*) and a perfect model (*L<sub>s</sub>*) according to  $D = -2 \left( \log \left( \frac{L_m}{L_s} \right) \right)$ . We computed the predictive ability of each model as the percent improvement of predictive deviance using 10-fold cross-validation over the null model, which can be interpreted as the percent variance explained when predicting to new data. Model goodness-of-fit was evaluated as the *R*<sup>2</sup> of a linear regression between observed and fitted CH<sub>4</sub> or CO<sub>2</sub> concentrations. To estimate model stability, each boosted regression tree model was run 10 times with different random seeds using a different subset of observations to train each model.

#### 2.4.3. Model Interpretation

An advantage of boosted regression tree models compared to other machine learning algorithms is the interpretability of the model results. The relative importance of each predictor variable can be calculated from the number of times it is selected for splitting in a decision tree, weighted by the improvement of the model caused by its inclusion, and then averaged over all trees in the final model. Variable relative importance is scaled to sum to 100. Individual conditional expectation plots and partial dependence plots are useful for visualizing heterogeneity in responses, interactions between predictors, and the average response to a predictor. Each line of an individual conditional expectation plot is calculated by varying the predictor of interest across the range of values in the training data set, while holding all other variables constant for that observation (Goldstein et al., 2015). Partial dependence plots are the average predicted response across observations of individual conditional expectation plots. We smoothed individual expectation and partial dependence plots using the loess method and set the *x*-axis limits to truncate the 10th and 90th percentile of observations to avoid over-interpretation (Goldstein et al., 2015). All partial dependence and individual conditional expectation plots are centered on 0 µM predicted CH<sub>4</sub> or CO<sub>2</sub>.

### 3. Results and Discussion

Waterbody dissolved CO<sub>2</sub> and CH<sub>4</sub> concentrations in the YK Delta were similar on average to those found in other studies of lakes in Alaska and the Northwest Territories of Canada, although we observed a wider range and greater variability for both CO<sub>2</sub> and CH<sub>4</sub> (Figure 2; Cunada et al., 2018; Stackpoole et al., 2017; Townsend-Small

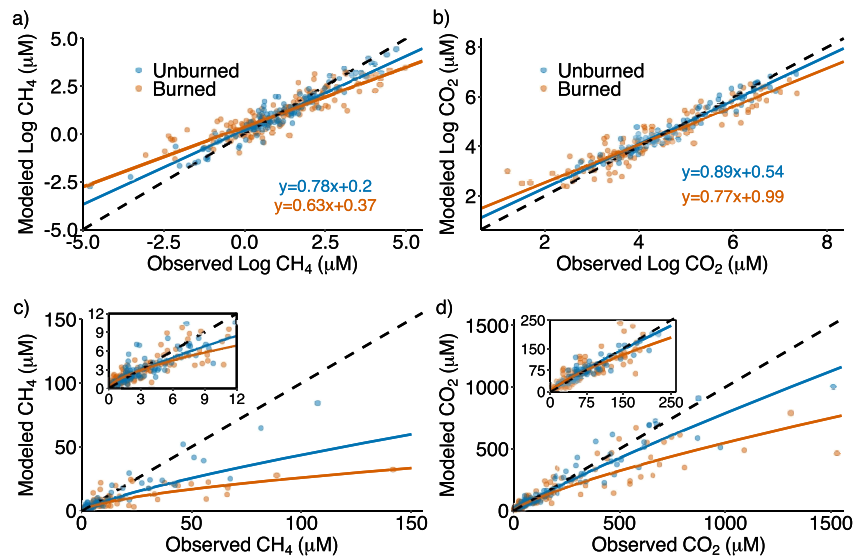


**Figure 3.** Modeled and observed dissolved gas concentrations for CH<sub>4</sub> (a and c) and CO<sub>2</sub> (b and d), unburned (blue) and burned (orange). Model goodness-of-fit shown using log-transformed data (a and b) and un-transformed data (c and d). One-to-one lines are the dashed lines, and linear regressions of fit are solid blue for unburned and orange for burned.

et al., 2017). Both the differences in CO<sub>2</sub> and CH<sub>4</sub> concentrations between waterbody types and the variability within waterbodies tended to be greater than the effects of fire on CO<sub>2</sub> and CH<sub>4</sub> concentrations (Figure 2). The effects of fire were inconsistent across waterbody types: for some fen surface waters, burned watersheds had higher CH<sub>4</sub> concentrations, but for lakes in burned watersheds, CH<sub>4</sub> concentrations were lower than in unburned watersheds. The boosted regression tree models predicted 79% and 52% of the observed variability in dissolved CO<sub>2</sub> and CH<sub>4</sub>, respectively in waterbodies from unburned watersheds, and predicted 61% and 36% of dissolved CO<sub>2</sub> and CH<sub>4</sub> in waterbodies from recently burned watersheds (Table 1).

### 3.1. Model Performance

The boosted regression tree models developed for burned and unburned watersheds were able to accurately model and predict dissolved CO<sub>2</sub> and CH<sub>4</sub> in waterbodies. Model fit was better for CO<sub>2</sub> than CH<sub>4</sub> and better for unburned than burned watersheds. The final number of variables retained in each model ranged from 13 to 18 (Table 1). The goodness-of-fits for all models were excellent, with  $R^2$  ranging from 0.79 to 0.94 (Table 1). Because the observations were log-transformed and the slopes of fit were all less than one (0.63–0.89), predicted values are conservative and in particular underestimated high concentrations of dissolved CO<sub>2</sub> and CH<sub>4</sub> (Figure 3). Model predictive ability (percent deviance explained) was better for aquatic systems within unburned than burned watersheds (Table 1). This disparity in performance could reflect processes that are important for regulating waterbody dissolved CO<sub>2</sub> and CH<sub>4</sub> in burned watersheds that were not measured in this study, such as increased thaw depths. Alternatively, a larger sample size might be needed for increased predictive performance for burned watersheds due to the range in contributing watershed area burned or heterogeneity in fire severity.

### 3.2. Drivers of Dissolved CO<sub>2</sub> and CH<sub>4</sub> in Waterbodies

#### 3.2.1. Effects of Waterbody Shape

Waterbody size and complexity of waterbody shape were the largest drivers of dissolved CO<sub>2</sub> and contributed 45% and 25% relative influence in unburned and burned watershed models respectively (Figure 4a). Waterbody shape variables contributed to explaining a small but significant portion (4%–5%) of CH<sub>4</sub> models (Figure 4b). We observed that smaller waterbodies had higher predicted dissolved CO<sub>2</sub> and CH<sub>4</sub> (Figures 4, 5b and 5d), which is consistent with the global pattern (Holgerson & Raymond, 2016). Higher dissolved CH<sub>4</sub> and CO<sub>2</sub> in small lakes have been attributed to high edge or sediment to water volume ratios and more frequent mixing of the water column (Bastviken et al., 2008). Predicted dissolved CH<sub>4</sub> and CO<sub>2</sub> increased as the area: perimeter ratio

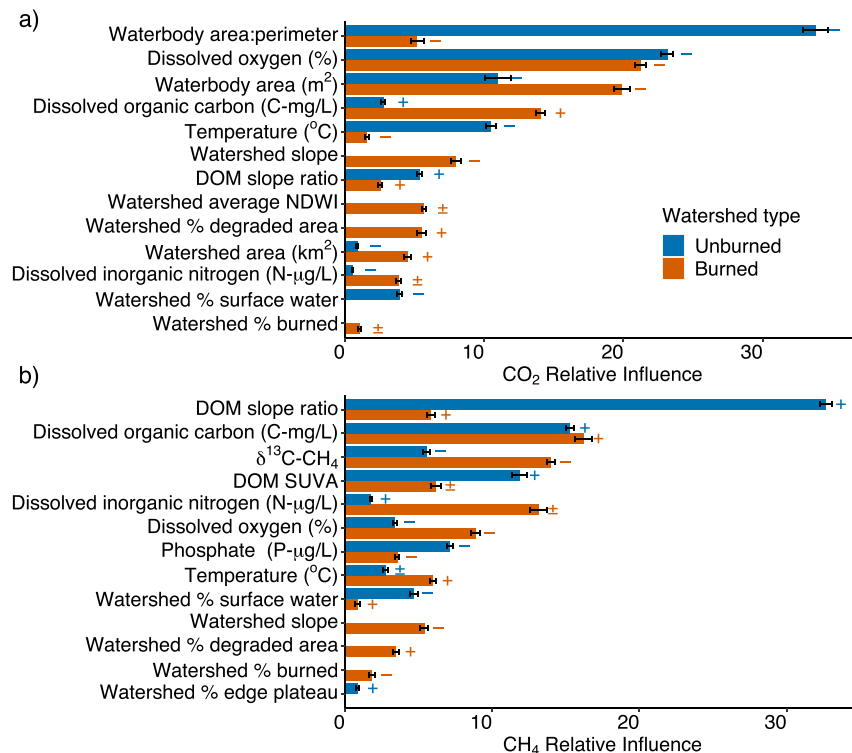


**Figure 4.** Relative influence of variables in unburned (blue) and burned (orange) watersheds in boosted regression tree models predicting CO<sub>2</sub> (a) and CH<sub>4</sub> (b) concentrations in waterbodies in the YK Delta of Alaska. The symbol labels indicate the overall effect of each predictor on CO<sub>2</sub> or CH<sub>4</sub>, whether positive (+), negative (−), or both (±). Error bars indicate standard deviation of relative influence from 10 boosted regression tree models run with different random seeds. Relative influences were scaled to 100%, with low influence predictors not depicted (a: waterbody area, waterbody area:perimeter, watershed area, waterbody pH, watershed NDWI, waterbody conductivity, b: waterbody pH, SUVA, phosphate concentration, conductivity). The full listing of variable relative influences can be found in Table S1 in Supporting Information S1.

decreased, supporting the role of edge effects (Figures 5a and 5c; Figure 4). Compared to the unburned model, the relative importance of waterbody area increased in the burned CO<sub>2</sub> model, whereas the relative importance of the area:perimeter ratio decreased. This would indicate that waterbodies in burned watersheds were less sensitive to near-shore edge effects than waterbodies in unburned watersheds, possibly due to changes in thaw depths, hydrology, or vegetation after fire in terrestrial-aquatic transitions at waterbody edges.

Terrestrial-aquatic transition zones, which are relatively more influential in smaller water bodies, have long been recognized as biogeochemical hot spots, where flowpaths converge to potentially supply substrates and conditions that promote disproportionately high reaction rates (Lin et al., 2012; McClain et al., 2003; Zhang et al., 2020). There are numerous mechanisms by which waterbody edges could support greater dissolved CO<sub>2</sub>. For example, complex lake shorelines are exposed to more latent heat than smooth shorelines, and could experience greater slumping and soil organic matter inputs from permafrost thaw. Alternatively, riparian and emergent vegetation at waterbody edges could influence the composition of soil porewater or hyporheic flowpaths. Our results are encouraging for applications scaling waterbody CO<sub>2</sub> concentrations, because, although more research is needed to clarify the role of waterbody edge effects in regulating CO<sub>2</sub> concentrations, waterbody size and shape are easy to measure with remote sensing and use as spatially-resolved drivers.

### 3.2.2. Effects of Carbon Composition and Quantity

The top three drivers of waterbody dissolved CH<sub>4</sub> in unburned watersheds were all related to carbon composition and together comprised 59% of the relative influence on dissolved CH<sub>4</sub>, while the remaining variables contributed ~5% or less each (Figure 4b). The highest relative influence predictor was DOM slope ratio, an indicator of carbon lability, at 32% (Figure 4b). DOC concentration was the next strongest predictor variable at 15%

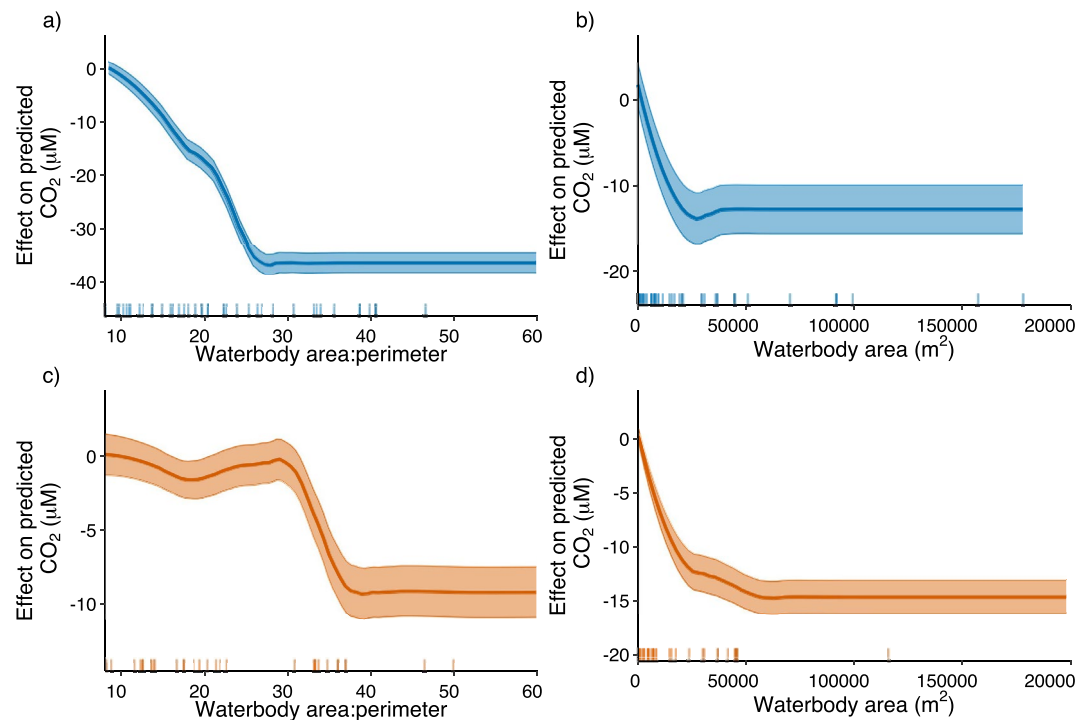


**Figure 5.** Partial dependence plots of the average effects of waterbody area/perimeter ratio (a and c) and waterbody area (b and d) on predicted carbon dioxide in unburned (blue) and burned (orange) watersheds. Shading indicates the standard deviation of the partial dependence functions from 10 boosted regression tree models run with different random seeds.

relative influence, followed by the SUVA of DOM, an indicator of carbon aromaticity, at 12% relative influence (Figure 4b).

The effects of DOC concentration and composition on waterbody dissolved CH<sub>4</sub> were generally positive, indicating that labile carbon sources might be limiting methanogenesis in unburned waterbodies (Figure 6c). Moreover, there was a strong interaction between DOC concentration and composition. When carbon composition was more unreactive (as derived from low slope ratio and high SUVA values), there was no effect of DOC on CH<sub>4</sub> at low concentrations, and a slight positive effect on CH<sub>4</sub> at high DOC concentrations (Figures 6a and 6b). When carbon composition was labile (as indicated by high slope ratio and low SUVA values) and carbon concentrations were low, there was a negative effect of DOC on CH<sub>4</sub>, likely demonstrating the inability of the energetically unfavorable metabolism of methanogens to compete for carbon (Figures 6a and 6b). When carbon compositions were labile and carbon concentrations were high (>10 mg/L), CH<sub>4</sub> concentrations increased rapidly with DOC concentration until plateauing at DOC concentrations of ~20 mg/L, where carbon may no longer be limiting (Figures 6a and 6b). Our findings are consistent with radiocarbon tracing studies in boreal fen peatlands that found dissolved CH<sub>4</sub> was mostly derived from labile DOM (Chanton et al., 2008), and with a study of lakes in the Mackenzie River Delta where dissolved CH<sub>4</sub> concentrations were also correlated with DOM slope ratio (Cunada et al., 2018). Our results indicate that in unburned waterbodies in the YK Delta, CH<sub>4</sub> concentrations were primarily controlled by carbon limitation (i.e., CH<sub>4</sub> concentrations were highest when there was abundant labile carbon).

DOM quality and availability were the dominant drivers in methane production in unburned watersheds, but clearly influenced respiration and methanogenesis in all waterbodies. While the effects of DOC and carbon composition were similar for dissolved CH<sub>4</sub> in burned watersheds (Figure 6d), the relative influence of carbon-related drivers was lower at 29% (Figure 4b). We would expect respiration from decomposition more generally, not just methanogenesis, to be driven by carbon substrate availability as well. While dissolved CO<sub>2</sub> in burned and unburned watersheds followed a similar pattern to that of CH<sub>4</sub> (i.e., increasing carbon availability and lability increased CO<sub>2</sub>; Figures 6e and 6f), the strengths of carbon-related drivers were lower, totaling 19% and 10% relative influence respectively (Figure 4a).

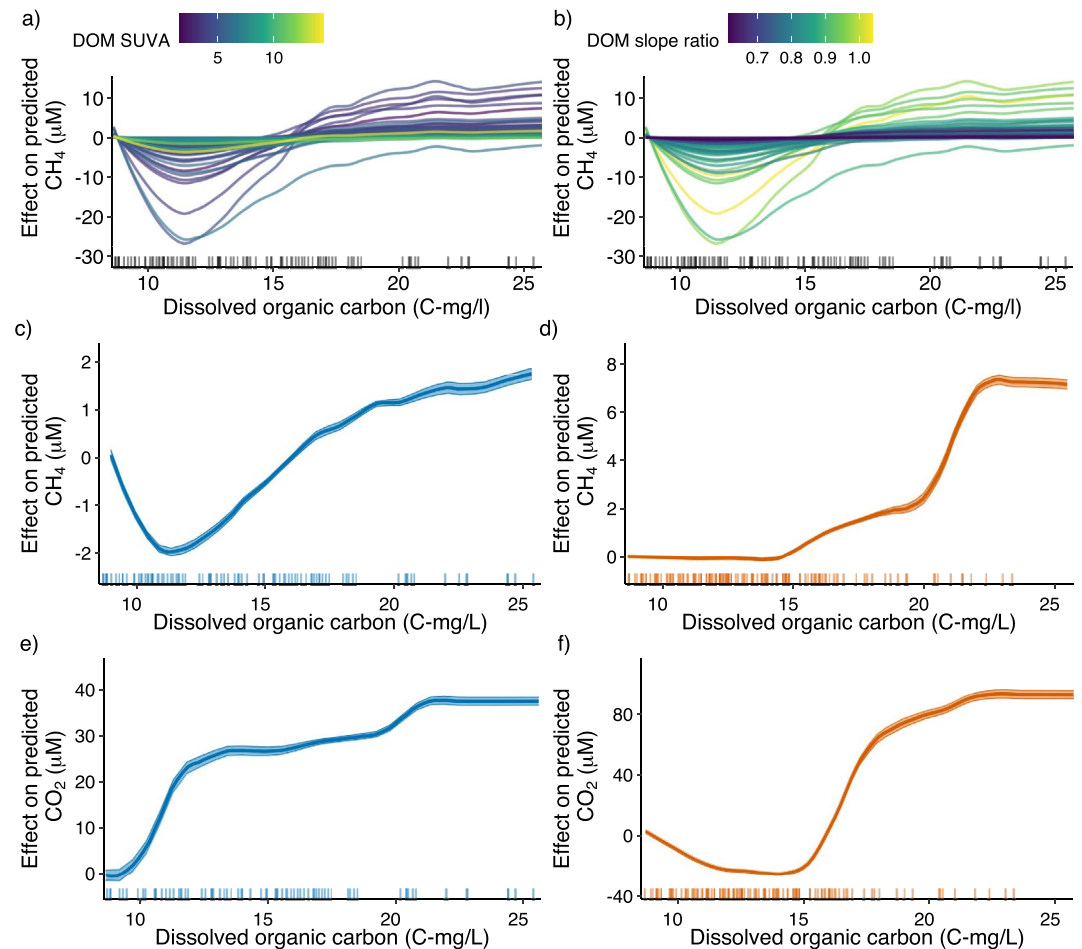


**Figure 6.** Effects of dissolved organic matter (DOM) quantity and composition on  $\text{CH}_4$  and  $\text{CO}_2$  concentrations in the Yukon-Kuskokwim Delta of Alaska. Top: individual conditional expectation plots of the effects of dissolved organic carbon concentrations (DOC) on predicted dissolved  $\text{CH}_4$  in unburned watersheds. Line color corresponds to dissolved organic matter Specific UV absorbance (SUVA) (a) and slope ratio (b). Partial dependence plots of the average effects of DOC on predicted  $\text{CH}_4$  in unburned (c) and burned (d) watersheds, and on predicted  $\text{CO}_2$  in unburned (e) and burned (f) watersheds.

### 3.2.3. Environmental Controls: Dissolved Oxygen, Temperature, and pH

Dissolved oxygen was one of the top drivers of waterbody dissolved  $\text{CO}_2$  in both burned and unburned with 21% and 23% relative influence respectively (Figure 4a). As dissolved oxygen increased, waterbody dissolved  $\text{CO}_2$  decreased, as expected for increased photosynthetic activity, decreased respiration, or greater exchange of  $\text{CO}_2$  with the atmosphere (Figures 7c and 7d). Warmer water temperatures and higher pH also were associated with lower  $\text{CO}_2$  concentrations, which is consistent both with primary productivity and respiration regulating  $\text{CO}_2$  concentrations (Figure 4, Figure S5g in Supporting Information S1). Chlorophyll-a concentrations and other gross primary productivity measurements have often been used as a proxy for dissolved  $\text{CO}_2$  in marine environments and large lakes (Chen et al., 2019; Landschützer et al., 2013). Even though the small lakes and other waterbodies in this study were all relatively high in DOC and likely net heterotrophic, our results indicate that primary productivity was important in regulating waterbody  $\text{CO}_2$  concentrations.

Dissolved oxygen and pH had a negative effect on dissolved  $\text{CH}_4$  in both burned and unburned watersheds (Figures 4, 7a and 7b, S31 in Supporting Information S1), which is consistent with low oxygen and pH being indicative of redox conditions suitable for methanogenesis and restrictive to methanotrophy (Meronigal et al., 2004; Segers, 1998). Temperature had an overall positive effect on predicted  $\text{CH}_4$  concentrations in water-

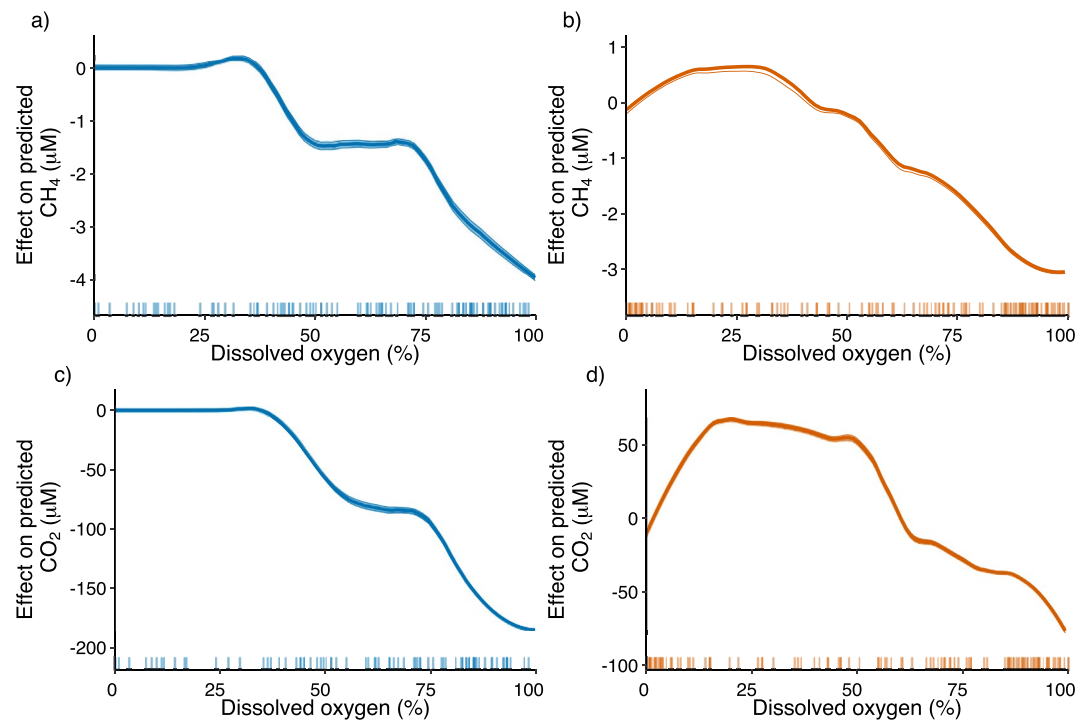


**Figure 7.** Partial dependence plots of the average effects of dissolved oxygen on predicted  $\text{CO}_2$  (c and d) and  $\text{CH}_4$  (a and b) in unburned (blue) and burned (orange) watersheds. Shading indicates the standard deviation of the partial dependence functions from 10 boosted regression tree models run with different random seeds.

bodies in burned and unburned watersheds, which is a typical metabolic response (Figure 4). In addition to the direct effects on metabolic rates, these environmental conditions can affect changes in microbial and methanogen community structure and methanogenesis pathways (Chowdhury et al., 2015; Jerman et al., 2009; Turetsky et al., 2008). Empirical relationships among dissolved oxygen and temperature are often used in models to scale up  $\text{CO}_2$  and  $\text{CH}_4$  emissions (Bridgham et al., 2013; Jiang et al., 2017; Lloyd & Taylor, 1994; Luus & Lin, 2015; Payn et al., 2014; Rinne et al., 2018; Ueyama et al., 2020; Yvon-Durocher et al., 2014; Zheng et al., 2018). However, temperature and dissolved oxygen only contributed 6% and 14% relative influence in the unburned and burned  $\text{CH}_4$  model (Figure 4b), indicating that typical scaling strategies for aquatic  $\text{CH}_4$  emissions could fall short for the YK Delta.

### 3.2.4. Effects of Nutrient Availability

Dissolved inorganic nitrogen had a small relative influence in both  $\text{CH}_4$  and  $\text{CO}_2$  unburned models, but 8-times greater influence in both burned models, while phosphate had a small but significant contribution to all models (Figure 4). The effects of dissolved inorganic nitrogen on dissolved  $\text{CH}_4$  and  $\text{CO}_2$  in burned watersheds were similar to each other. There was an initial negative relationship spanning the low range of concentrations (0–40  $\mu\text{g-N L}^{-1}$ ; Figures 8b and 8d). For nitrogen concentrations greater than median value in unburned watersheds (~40  $\mu\text{g-N L}^{-1}$ ; Figures 8a and 8c), the relationship reversed and both dissolved  $\text{CH}_4$  and  $\text{CO}_2$  increased with nitrogen availability until plateauing for nitrogen concentrations higher than 100  $\mu\text{g-N L}^{-1}$  (Figures 8b and 8d). Increased nitrogen leaching following wildfires has been observed in other arctic ecosystems, with more severe fires causing greater mobilization of nitrogen to downstream ecosystems (Abbott et al., 2021; Ludwig et al., 2018). The contrasting effects of nitrogen on dissolved  $\text{CH}_4$  and  $\text{CO}_2$  we observed could depend on the extent and severity of fire in a watershed; the high-N positive effect occurring when there was a large proportion of high severity burns in the watershed, and the low-N negative relationship when low severity burns were more abundant in the watershed.

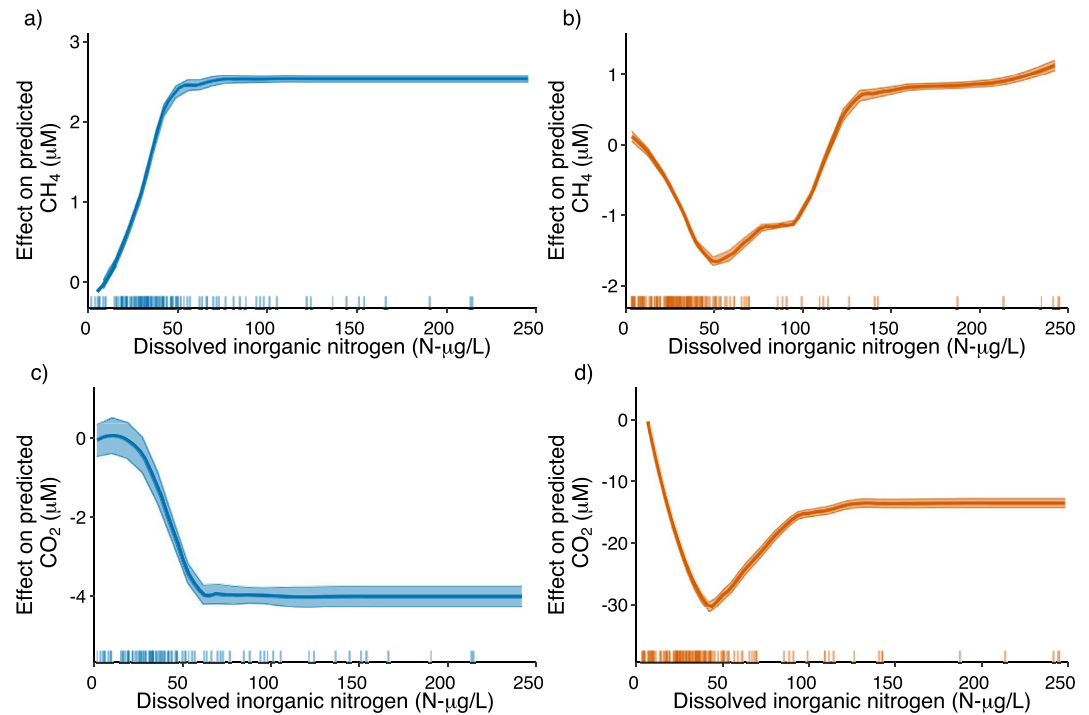


**Figure 8.** Partial dependence plots of the average effects of dissolved inorganic nitrogen on predicted CH<sub>4</sub> (a and b) and CO<sub>2</sub> concentrations (c and d) in unburned watersheds (blue) and burned watersheds (orange). Shading indicates the standard deviation of the partial dependence functions from 10 boosted regression tree models run with different random seeds.

A shift in the microbial community in burned watersheds could explain the observed changes in the effects of nitrogen. Both methanogenic and methanotrophic activity have been shown to increase in response to nutrient fertilization, with both positive, negative, and neutral net effects on CH<sub>4</sub> emissions (Aerts & Toet, 1997; Juutinen et al., 2018; Keller et al., 2005; Lund et al., 2009; Torn & Chapin, 1993; Veraart et al., 2015). This mechanism is supported by the increase in the relative influence of  $\delta^{13}\text{C}\text{-CH}_4$  from 6% in unburned watersheds to 14% in burned watersheds (Figure 4b). For both burned and unburned, CH<sub>4</sub> concentrations declined as the influence of methanotrophy increased, though the correlation in burned observations was stronger (Figure 4). The increased importance of  $\delta^{13}\text{C}\text{-CH}_4$  in burned waterbodies could indicate greater control of the microbial community through the balance of methanogenesis and methanotrophy.

### 3.2.5. Watershed Drivers

Upstream watersheds can directly influence CH<sub>4</sub> and CO<sub>2</sub> concentrations if hydrologic inputs (i.e., upstream waterbodies, sub- and supra-permafrost groundwater) have different concentrations than the water column (Dabrowski et al., 2020) and can indirectly influence CH<sub>4</sub> and CO<sub>2</sub> production in the water column by changing environmental constraints or supplying limiting reactants (McClain et al., 2003). Remotely-sensed watershed drivers (i.e., watershed slope, watershed size, percent area of degraded peat plateau) contributed a large portion of the explained variance in burned models for dissolved CH<sub>4</sub> and CO<sub>2</sub> (total 17% and 27% respectively) but contributed less to the unburned models for dissolved CH<sub>4</sub> and CO<sub>2</sub> (total 10% and 5% respectively; Figure 4). Percent area of surface water and watershed size had a positive effect on waterbody CH<sub>4</sub> and CO<sub>2</sub> concentrations in burned watersheds but a negative effect on downstream waterbody CH<sub>4</sub> and CO<sub>2</sub> concentrations in unburned watersheds (Figure 4). Upstream networks of waterbodies were thus more likely to be a source of dissolved CO<sub>2</sub> and CH<sub>4</sub> in burned watersheds, but dilute CH<sub>4</sub> and CO<sub>2</sub> concentrations in unburned watersheds. Percent area of peat plateau edges had a positive effect on CH<sub>4</sub> in unburned watershed (Figure 4) and degraded peat plateau had positive effects on dissolved CH<sub>4</sub> in burned watersheds (Figure 9a). Degraded peat plateau had a similar effect on dissolved CO<sub>2</sub> (Figure 9b), but edge plateau area was not retained as a driver in the CO<sub>2</sub> models. These ecosystem margins and disturbed areas could be hot spots of CH<sub>4</sub> and to a lesser extent CO<sub>2</sub> production, leading to greater soil pore and ground water inputs from

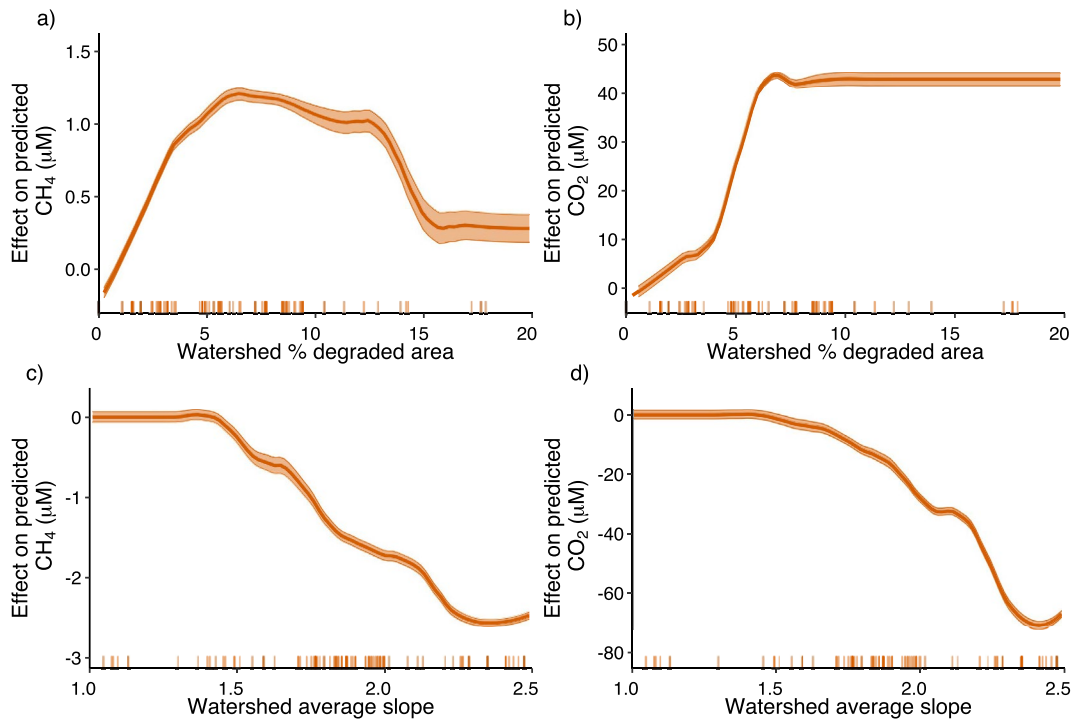


**Figure 9.** Partial dependence plots of the average effects of the percent of watershed area that is degraded permafrost (a and b) and watershed slope (c and d) on predicted CO<sub>2</sub> (b and d) and CH<sub>4</sub> (a and c) concentrations in burned watersheds. Shading indicates the standard deviation of the partial dependence functions from 10 boosted regression tree models run with different random seeds. Neither “watershed % degraded area” or “watershed average slope” were retained as variables in models for unburned watersheds.

the watershed. The average watershed slope had a negative effect on waterbody CH<sub>4</sub> and CO<sub>2</sub> concentrations, but was only a significant driver in burned watershed models and was not retained as a driver in unburned models (Figures 9c and 9d). Flatter watersheds could have longer water residence times, leading to increased leaching of DOM, more anoxia in pore water, and more reaction time for decomposition and respiration (Harms & Jones, 2012; Harms & Ludwig, 2016; Johnston et al., 2020; Judd & Kling, 2002; Koch et al., 2013; Newman et al., 2015; Olefeldt & Roulet, 2012; Throckmorton et al., 2015; Zarnetske et al., 2011). Our results demonstrate a shift away from waterbody edge effects and towards greater landscape connectivity and watershed level influences driving CO<sub>2</sub> and CH<sub>4</sub> concentrations in burned watersheds.

The percent area of a watershed that actually burned was a relevant driver in both CH<sub>4</sub> and CO<sub>2</sub> burned models. There was a threshold effect; percent watershed area burned did not affect CH<sub>4</sub> and CO<sub>2</sub> concentrations until greater than 65% of the watershed area was burned (Figures S4n and S6o in Supporting Information S1). This could suggest that more thoroughly burned watersheds affect dissolved CH<sub>4</sub> and CO<sub>2</sub> through variables we did not measure in this study. Watershed average NDWI, a metric associated with canopy wetness and soil moisture, was negatively correlated with percent burned area (Pearson correlation =  $-0.68$ ), indicating wetter conditions in partially burned watersheds than in complete burns. This could be driven by the absence of moss and other vegetation biomass in burned areas or an increased presence of higher severity burns with drier conditions. NDWI was a more important driver in burned than unburned models and had a bimodal effect on waterbody CH<sub>4</sub> and CO<sub>2</sub> concentrations; the highest concentrations occurred in the wettest conditions when NDWI was high and when NDWI values were lower than any of those found in unburned areas, which could be indicative of high severity burns (Figures S4k and S6e in Supporting Information S1). Our results demonstrate that the pattern of a fire, that is, whether watersheds were partially burned or completely burned can regulate the effects of fire on downstream waterbody chemistry, reinforcing the need for a landscape approach to predicting waterbody CH<sub>4</sub> and CO<sub>2</sub> concentrations.

### 3.3. Consequences of Fire for Waterbody CO<sub>2</sub> and CH<sub>4</sub> Concentrations and Scaling

Averaging across all waterbodies, there was no detectable difference between CH<sub>4</sub> and CO<sub>2</sub> concentrations in burned watersheds. However, the mechanisms driving dissolved CH<sub>4</sub> and CO<sub>2</sub> changed as a consequence of fire. Fire reduced the influence of DOM on dissolved CH<sub>4</sub> but increased the influence of DOM on dissolved CO<sub>2</sub>, with potentially balanced impacts on carbon emissions from waterbodies. The spatial extent of watershed burned area directly influenced dissolved CH<sub>4</sub> and CO<sub>2</sub>, and while we did not directly account for fire severity, it may have indirectly affected dissolved CH<sub>4</sub> and CO<sub>2</sub> through inorganic nitrogen availability and watershed soil and canopy moisture (NDWI). Fire increased the sensitivity of CH<sub>4</sub> and CO<sub>2</sub> concentrations in waterbodies to watershed landscape drivers (i.e., watershed slope, size, NDWI, percent area degraded permafrost) compared to near-shore effects (i.e., perimeter:area ratio) and internal waterbody mechanisms (i.e., DOM composition). Fire can affect hydrologic regimes in a number of ways, such as increasing thaw depths, deepening flowpaths, increasing the hydrophobicity of soils, increasing small wetland and pond formation through subsidence, or altering the water balance as a result of changes in evapotranspiration from recovering vegetation (Brown et al., 2015; Helbig et al., 2016; Michaelides et al., 2019; Petrone et al., 2007). While we do not have direct measurements of these mechanisms, these results suggest that waterbody CH<sub>4</sub> and CO<sub>2</sub> concentrations were more sensitive to watershed dynamics in burned watersheds. An integrated terrestrial-aquatic approach in fire-affected, wetland-dense, ecosystems could improve scaling of CH<sub>4</sub> and CO<sub>2</sub> emissions and reduce uncertainty in bottom-up estimates of the inland aquatic carbon budget.

## 4. Conclusions

The boosted regression tree models were able to depict well-documented ecological dynamics, such as temperature sensitivity and carbon limitation of microbial respiration and methanogenesis. The models were consistent with globally-observed patterns, such as the relationship between lake size and dissolved CH<sub>4</sub> and CO<sub>2</sub>, and were able to capture non-linear and interactive effects of predictor variables. Given that small waterbodies had the largest concentrations of CH<sub>4</sub> and CO<sub>2</sub>, accurately accounting for carbon emissions from these small but abundant sources could greatly reduce the uncertainty in inland aquatic carbon budgets. For example, dissolved CO<sub>2</sub> was largely driven by waterbody size and shape and was saturated with respect to the atmosphere, suggesting that these waterbodies could be a net source of CO<sub>2</sub> emissions, even during the peak growing season. However, these inland water bodies are largely attributed a flux of zero in top-down carbon budgets from atmospheric inversion models for example, Commane et al., 2017. More seasonal observations of inland aquatic CH<sub>4</sub> and CO<sub>2</sub> concentrations are needed to extend predictive models outside of the peak growing season.

Contrary to many empirical studies and process-based models, our results suggest that dissolved CH<sub>4</sub> concentrations were predominantly predicted by carbon availability and quality, as opposed to temperature and dissolved oxygen. However, our sampling regime was not designed to test temperature or oxygen dependence. Remote sensing of chromophoric DOM has been used to predict DOC concentrations in inland waters (Brezonik et al., 2015; Griffin et al., 2018; Kutser et al., 2005), and, though associated with greater uncertainty in complex inland waters with high carbon concentrations, this could be a fruitful avenue for mapping carbon availability and scaling CH<sub>4</sub> emissions in waterbodies in the YK Delta.

Our results suggest wildfires alter lake and wetland ecosystems in the YK Delta to be more sensitive to watershed landscape drivers. After fires, areas of degraded permafrost increased CH<sub>4</sub> and CO<sub>2</sub> concentrations in downstream waterbodies, contributing to a positive feedback to climate as the Arctic continues to warm and permafrost thaws. As wildfires increase in frequency and severity with climate change, it will become more important to use an integrated terrestrial-aquatic approach when scaling inland aquatic carbon fluxes.

### Data Availability Statement

The surface water chemistry and environmental data used in the boosted regression tree models in this study are available at the Arctic Data Center repository via <http://doi.org/10.18739/A22804Z8M> and <http://doi.org/10.18739/A23775V7T>.

### Acknowledgments

I would like to acknowledge that our research work took place on the traditional land of the Yup'ik, who have stewarded this land through many generations. Our work would not have been possible without the support of the Yukon Delta National Wildlife Refuge, U.S. Fish and Wildlife Service. This study was supported with funding from a National Aeronautics and Space Administration FINESST grant (80NSSC19K1301) to S.M.L. and National Science Foundation grants (NSF-1044610 and NSF-1561437) to S.M.N. This work would not have been possible without the efforts of the Polarix Project undergraduate students from 2017 to 2019 in sample collection and processing. The maps in Figures 1 and S1 in Supporting Information S1 were created by Meghan Jones.

### References

- Abbott, B. W., Rocha, A. V., Shogren, A., Zarnetske, J. P., Iannucci, F., Bowden, W. B., et al. (2021). Tundra wildfire triggers sustained lateral nutrient loss in Alaskan Arctic. *Global Change Biology*, 27(7), 1408–1430. <https://doi.org/10.1111/gcb.15507>
- Aerts, R., & Toet, S. (1997). Nutritional controls on carbon dioxide and methane emission from Carex-dominated peat soils. *Soil Biology and Biochemistry*, 29(11–12), 1683–1690. [https://doi.org/10.1016/s0038-0717\(97\)00073-4](https://doi.org/10.1016/s0038-0717(97)00073-4)
- Alexander, H. D., Natali, S. M., Loranty, M. M., Ludwig, S. M., Spektor, V. V., Davydov, S., et al. (2018). Impacts of increased soil burn severity on larch forest regeneration on permafrost soils of for northeastern Siberia. *Forest Ecology and Management*, 417, 144–153. <https://doi.org/10.1016/j.foreco.2018.03.008>
- Bartlett, K. B., Crill, P. M., Sass, R. L., Harriss, R. C., & Dise, N. B. (1992). Methane emissions from tundra environments in the Yukon-Kuskokwim Delta, Alaska. *Journal of Geophysical Research*, 97(D15), 16645–16660. <https://doi.org/10.1029/91jd00610>
- Bastviken, D., Cole, J. J., Pace, M. L., & de Bogert, M. C. V. (2008). Fates of methane from different lake habitats: Connecting whole-lake budgets and CH<sub>4</sub> emissions. *Journal of Geophysical Research*, 113, G02024. <https://doi.org/10.1029/2007jg000608>
- Bastviken, D., Tranvik, L. J., Downing, J. A., Crill, P. M., & Enrich-prast, A. (2011). Freshwater methane emissions offset the continental carbon sink. *Science*, 331, 50. <https://doi.org/10.1126/science.1196808>
- Belshe, E. F., Schuur, E. A. G., & Bolker, B. M. (2013). Tundra ecosystems observed to be CO<sub>2</sub> sources due to differential amplification of the carbon cycle. *Ecology Letters*, 16(10), 1307–1315. <https://doi.org/10.1111/ele.12164>
- Boby, L. A., Schuur, E. A. G., Mack, M. C., Verbyla, D., & Johnstone, J. F. (2010). Quantifying fire severity, carbon, and nitrogen emissions in Alaska's boreal forest. *Ecological Applications*, 20(6), 1633–1647. <https://doi.org/10.1890/08-2295.1>
- Bond-Lamberty, B., Peckham, S. D., Ahl, D. E., & Gower, S. T. (2007). Fire as the dominant driver of central Canadian boreal forest carbon balance. *Nature*, 450(7166), 89–92. <https://doi.org/10.1038/nature06272>
- Bond-Lamberty, B., Wang, C., & Gower, S. T. (2004). Net primary production and net ecosystem production of a boreal black spruce wildfire chronosequence. *Global Change Biology*, 10(4), 473–487. <https://doi.org/10.1111/j.1529-8817.2003.0742.x>
- Boucher, O., Friedlingstein, P., Collins, B., & Shine, K. P. (2009). The indirect global warming potential and global temperature change potential due to methane oxidation. *Environmental Research Letters*, 4(4), 044007. <https://doi.org/10.1088/1748-9326/4/4/044007>
- Brezonik, P. L., Olmanson, L. G., Finlay, J. C., & Bauer, M. E. (2015). Factors affecting the measurement of CDOM by remote sensing of optically complex inland waters. *Remote Sensing of Environment*, 157, 199–215. <https://doi.org/10.1016/j.rse.2014.04.033>
- Bridgman, S. D., Cadillo-Quiroz, H., Keller, J., & Zhuang, Q. (2013). Methane emissions from wetlands: Biogeochemical, microbial, and modeling perspectives from local to global scales. *Global Change Biology*, 19(5), 1325–1346. <https://doi.org/10.1111/gcb.12131>
- Brown, D. R. N., Jorgenson, M. T., Douglas, T. A., Romanovsky, V. E., Kielland, K., Hiemstra, C., et al. (2015). Interactive effects of wildfire and climate on permafrost degradation in Alaskan lowland forests. *Journal of Geophysical Research: Biogeosciences*, 120, 1619–1637. <https://doi.org/10.1002/2015jg003033>
- Chang, R. Y.-W., Miller, C. E., Dinardo, S. J., Karion, A., Sweeney, C., Daube, B. C., et al. (2014). Methane emissions from Alaska in 2012 from CARVE airborne observations. *Proceedings of the National Academy of Sciences*, 111, 16694–16699. <https://doi.org/10.1073/pnas.1412953111>
- Chanton, J. P., Glaser, P. H., Chasar, L. S., Burdige, D. J., Hines, M. E., Siegel, D. I., et al. (2008). Radiocarbon evidence for the importance of surface vegetation on fermentation and methanogenesis in contrasting types of boreal peatlands. *Global Biogeochemical Cycles*, 22, GB4022. <https://doi.org/10.1029/2008gb003274>
- Chapin, F. I., & Woodwell, G. (2006). Reconciling carbon-cycle concepts, terminology, and methods. *Ecosystems*, 9, 1041–1050. <https://doi.org/10.1007/s10021-005-0105-7>
- Chen, S., Hu, C., Barnes, B. B., Wanninkhof, R., Cai, W.-J., Barbero, L., & Pierrot, D. (2019). A machine learning approach to estimate surface ocean pCO<sub>2</sub> from satellite measurements. *Remote Sensing of Environment*, 228, 203–226. <https://doi.org/10.1016/j.rse.2019.04.019>
- Chen, X., Bohn, T. J., & Lettenmaier, D. P. (2015). Model estimates of climate controls on pan-Arctic wetland methane emissions. *Biogeosciences*, 12, 6259–6277. <https://doi.org/10.5194/bg-12-6259-2015>
- Chowdhury, T. R., Herndon, E. M., Phelps, T. J., Elias, D. A., Gu, B., Liang, L., et al. (2015). Stoichiometry and temperature sensitivity of methanogenesis and CO<sub>2</sub> production from saturated polygonal tundra in Barrow, Alaska. *Global Change Biology*, 21, 722–737. <https://doi.org/10.1111/gcb.12762>
- Clewley, D., Whitcomb, J., Moghaddam, M., McDonald, K., Chapman, B., & Bunting, P. (2015). Evaluation of ALOS PALSAR data for high-resolution mapping of vegetated wetlands in Alaska. *Remote Sensing*, 7, 7272–7297. <https://doi.org/10.3390/rs70607272>
- Cole, J. J., Prairie, Y. T., Caraco, N. F., McDowell, W. H., Tranvik, L. J., Striegl, R. G., et al. (2007). Plumbing the global carbon cycle: Integrating inland waters into the terrestrial carbon budget. *Ecosystems*, 10, 172–185. <https://doi.org/10.1007/s10021-006-9013-8>
- Commans, R., Lindaas, J., Benmergui, J., Luus, K. A., Chang, R. Y.-W., Daube, B. C., et al. (2017). Carbon dioxide sources from Alaska driven by increasing early winter respiration from Arctic tundra. *Proceedings of the National Academy of Sciences*, 114, 5361–5366. <https://doi.org/10.1073/pnas.1618567114>
- Cunada, C. L., Lesack, L. F. W., & Tank, S. E. (2018). Seasonal dynamics of dissolved methane in lakes of the Mackenzie Delta and the role of carbon substrate quality. *Journal of Geophysical Research: Biogeosciences*, 123, 591–609. <https://doi.org/10.1002/2017jg004047>
- Dabrowski, J. S., Charette, M. A., Mann, P. J., Ludwig, S. M., Natali, S. M., Holmes, R. M., et al. (2020). Using radon to quantify groundwater discharge and methane fluxes to a shallow, tundra lake on the Yukon-Kuskokwim Delta. *Biogeochemistry*, 148, 69–89. <https://doi.org/10.1007/s10533-020-00647-w>
- Dooley, S. R., & Treseder, K. K. (2011). The effect of fire on microbial biomass: A meta-analysis of field studies. *Biogeochemistry*, 109, 49–61. <https://doi.org/10.1007/s10533-011-9633-8>
- Elith, J., Leathwick, J. R., & Hastie, T. (2008). A working guide to boosted regression trees. *Journal of Animal Ecology*, 77, 802–813. <https://doi.org/10.1111/j.1365-2656.2008.01390.x>
- Fan, S. M., Wofsy, S. C., Bakwin, P. S., Jacob, D. J., Anderson, S. M., Kebejian, P. L., et al. (1992). Micrometeorological measurements of CH<sub>4</sub> and CO<sub>2</sub> exchange between the atmosphere and subarctic tundra. *Journal of Geophysical Research*, 97, 16627–16643. <https://doi.org/10.1029/91jd02531>
- Goldstein, A., Kapelner, A., Bleich, J., & Pitkin, E. (2015). Peeking inside the black box: Visualizing statistical learning with plots of individual conditional expectation. *Journal of Computational & Graphical Statistics*, 24, 44–65. <https://doi.org/10.1080/10618600.2014.907095>
- Griffin, C. G., McClelland, J. W., Frey, K. E., Fiske, G., & Holmes, R. M. (2018). Quantifying CDOM and DOC in major Arctic rivers during ice-free conditions using Landsat TM and ETM+ data. *Remote Sensing of Environment*, 209, 395–409. <https://doi.org/10.1016/j.rse.2018.02.060>

- Harms, T. K., & Jones, J. B. (2012). Thaw depth determines reaction and transport of inorganic nitrogen in valley bottom permafrost soils. *Global Change Biology*, *18*, 2958–2968. <https://doi.org/10.1111/j.1365-2486.2012.02731.x>
- Harms, T. K., & Ludwig, S. M. (2016). Retention and removal of nitrogen and phosphorus in saturated soils of arctic hillslopes. *Biogeochemistry*, *127*, 291–304. <https://doi.org/10.1007/s10533-016-0181-0>
- Helbig, M., Pappas, C., & Sonnentag, O. (2016). Permafrost thaw and wildfire: Equally important drivers of boreal tree cover changes in the Taiga Plains, Canada. *Geophysical Research Letters*, *43*, 1598–1606. <https://doi.org/10.1002/2015gl067193>
- Helms, J. R., Stubbins, A., Ritchie, J. D., Minor, E. C., Kieber, D. J., & Mopper, K. (2008). Absorption spectral slopes and slope ratios as indicators of molecular weight, source, and photobleaching of chromophoric dissolved organic matter. *Limnology & Oceanography*, *53*, 955–969. <https://doi.org/10.4319/lo.2008.53.3.0955>
- Holgerson, M. A., & Raymond, P. A. (2016). Large contribution to inland water CO<sub>2</sub> and CH<sub>4</sub> emissions from very small ponds. *Nature Geoscience*, *9*, 222–226. <https://doi.org/10.1038/ngeo2654>
- Hotchkiss, E. R., Hall, R. O., Jr., Sponseller, R. A., Butman, D., Klaminder, J., Laudon, H., et al. (2015). Sources of and processes controlling CO<sub>2</sub> emissions change with the size of streams and rivers. *Nature Geoscience*, *8*, 696–699. <https://doi.org/10.1038/ngeo2507>
- Hugelius, G., Loisel, J., Chadburn, S., Jackson, R. B., Jones, M., MacDonald, G., et al. (2020). Large stocks of peatland carbon and nitrogen are vulnerable to permafrost thaw. *Proceedings of the National Academy of Sciences*, *117*, 20438–20446. <https://doi.org/10.1073/pnas.1916387117>
- Hugelius, G., Strauss, J., Zubrzycki, S., Harden, J. W., Schuur, E. A. G., Ping, C. L., et al. (2014). Improved estimates show large circumpolar stocks of permafrost carbon while quantifying substantial uncertainty ranges and identifying remaining data gaps. *Biogeosciences Discussions*, *11*, 4771–4822. <https://doi.org/10.5194/bg-11-6573-2014>
- Hutchins, R. H. S., Tank, S. E., Olefeldt, D., Quinton, W. L., Spence, C., Dion, N., et al. (2020). Fluvial CO<sub>2</sub> and CH<sub>4</sub> patterns across wildfire-disturbed ecozones of subarctic Canada: Current status and implications for future change. *Global Change Biology*, *26*, 2304–2319. <https://doi.org/10.1111/gcb.14960>
- IPCC (2013). Climate Change 2013: The physical science basis. In S. Solomon, D. Qin, M. Manning, Z. Chen, M. Marquis, K. B. Averyt, M. Tignor, & H. L. Miller (Eds.), *Contribution of working group I to the fifth assessment report of the intergovernmental panel on climate change*. Cambridge University Press.
- Jerman, V., Metje, M., & Mandi, I. (2009). Wetland restoration and methanogenesis: The activity of microbial populations and competition for substrates at different temperatures. *Biogeosciences*, *6*, 1127–1138. <https://doi.org/10.5194/bg-6-1127-2009>
- Jiang, Y., Rastetter, E. B., Shaver, G. R., Rocha, A. V., Zhuang, Q., & Kwiatkowski, B. L. (2017). Modeling long-term changes in tundra carbon balance following wildfire, climate change, and potential nutrient addition. *Ecological Applications*, *27*, 105–117. <https://doi.org/10.1002/eap.1413>
- Johnston, S. E., Striegl, R. G., Bogard, M. J., Dornblaser, M. M., Butman, D. E., Kellerman, A. M., et al. (2020). Hydrologic connectivity determines dissolved organic matter biogeochemistry in northern high-latitude lakes. *Limnology & Oceanography*, *65*, 1764–1780. <https://doi.org/10.1002/lno.11417>
- Jorgenson, M. T., & Osterkamp, T. E. (2005). Response of boreal ecosystems to varying modes of permafrost degradation. *Canadian Journal of Forest Research*, *35*, 2100–2111. <https://doi.org/10.1139/x05-153>
- Jorgenson, M. T., Romanovsky, V., Harden, J., Shur, Y., Donnell, J. O., Schuur, E. A. G., & Kanevskiy, M. (2010). Resilience and vulnerability of permafrost to climate change. *Canadian Journal of Forest Research*, *40*, 1219–1236. <https://doi.org/10.1139/x10-060>
- Judd, K. E., & Kling, G. W. (2002). Production and export of dissolved C in arctic tundra mesocosms: The roles of vegetation and water flow. *Biogeochemistry*, *60*, 213–234. <https://doi.org/10.1023/a:1020371412061>
- Juutinen, S., Moore, T. R., Bubier, J. L., Arnkil, S., Humphreys, E., Marincak, B., et al. (2018). Long-term nutrient addition increased CH<sub>4</sub> emission from a bog through direct and indirect effects. *Scientific Reports*, *8*, 3838. <https://doi.org/10.1038/s41598-018-22210-2>
- Kasischke, E. S., Verbyla, D. L., Rupp, T. S., McGuire, A. D., Murphy, K. A., Jandt, R., et al. (2010). Alaska's changing fire regime—Implications for the vulnerability of its boreal forests. *Canadian Journal of Forest Research*, *40*, 1313–1324. <https://doi.org/10.1139/x10-098>
- Keller, J. K., Bridgman, S. D., Chapin, C. T., & Iversen, C. M. (2005). Limited effects of six years of fertilization on carbon mineralization dynamics in a Minnesota fen. *Soil Biology and Biochemistry*, *37*, 1197–1204. <https://doi.org/10.1016/j.soilbio.2004.11.018>
- Kling, G. W., Kipphut, G. W., & Miller, M. C. (1991). Lakes and streams for tundra carbon budgets atmosphere: Implications. *Science*, *251*, 298–301. <https://doi.org/10.1126/science.251.4991.298>
- Koch, J. C., Runkel, R. L., Striegl, R., & McKnight, D. M. (2013). Hydrologic controls on the transport and cycling of carbon and nitrogen in a boreal catchment underlain by continuous permafrost. *Journal of Geophysical Research: Biogeosciences*, *118*, 698–712. <https://doi.org/10.1002/jgrg.20058>
- Kutser, T., Pierson, D. C., Kallio, K. Y., Reinart, A., & Sobek, S. (2005). Mapping lake CDOM by satellite remote sensing. *Remote Sensing of Environment*, *94*, 535–540. <https://doi.org/10.1016/j.rse.2004.11.009>
- Landschützer, P., Gruber, N., Bakker, D. C. E., Schuster, U., Nakaoka, S., Payne, M., et al. (2013). A neural network-based estimate of the seasonal to inter-annual variability of the Atlantic Ocean carbon sink. *Biogeosciences*, *10*, 8799–8849. <https://doi.org/10.5194/bg-10-8799-2013>
- Lapierre, J.-F., & del Giorgio, P. A. (2012). Geographical and environmental drivers of regional differences in the lake pCO<sub>2</sub> versus DOC relationship across northern landscapes. *Journal of Geophysical Research*, *117*, G03015. <https://doi.org/10.1029/2012jg001945>
- Lin, X., Green, S., Tfaily, M. M., Prakash, O., Konstantinidis, K. T., Corbett, J. E., et al. (2012). Microbial community structure and activity linked to contrasting biogeochemical gradients in bog and fen environments of the Glacial Lake Agassiz Peatland. *Applied and Environmental Microbiology*, *78*, 7023–7031. <https://doi.org/10.1128/aem.01750-12>
- Lloyd, J., & Taylor, J. a. (1994). On the temperature dependence of soil respiration. *Functional Ecology*, *8*, 315. <https://doi.org/10.2307/2389824>
- Ludwig, S. M., Alexander, H. D., Kielland, K., Mann, P. J., Natali, S. M., & Ruess, R. W. (2018). Fire severity effects on soil carbon and nutrients and microbial processes in a Siberian larch forest. *Global Change Biology*, 5841–5852. <https://doi.org/10.1111/gcb.14455>
- Lund, M., Christensen, T. R., Mastepanov, M., Lindroth, A., & Ström, L. (2009). Effects of N and P fertilization on the greenhouse gas exchange in two northern peatlands with contrasting N deposition rates. *Biogeosciences*, *6*, 2135–2144. <https://doi.org/10.5194/bg-6-2135-2009>
- Luus, K. A., & Lin, J. C. (2015). The polar vegetation photosynthesis and respiration model: A parsimonious, satellite-data-driven model of high-latitude CO<sub>2</sub> exchange. *Geoscientific Model Development*, *8*, 2655–2674. <https://doi.org/10.5194/gmd-8-2655-2015>
- Mack, M. C., Treseder, K. K., Manies, K. L., Harden, J. W., Schuur, E. A. G., Vogel, J. G., et al. (2008). Recovery of aboveground plant biomass and productivity after fire in mesic and dry black spruce forests of interior Alaska. *Ecosystems*, *11*, 209–225. <https://doi.org/10.1007/s10021-007-9117-9>
- McClain, M. E., Boyer, E. W., Dent, C. L., Gergel, S. E., Grimm, N. B., Groffman, P. M., et al. (2003). Biogeochemical hot spots and hot moments at the interface of terrestrial and aquatic ecosystems. *Ecosystems*, *6*, 301–312. <https://doi.org/10.1007/s10021-003-0161-9>
- Megonigal, J. P., Hines, M. E., & Visscher, P. T. (2004). Anaerobic metabolism: Linkages to Trace gases and aerobic processes. In W. H. Schlesinger (Ed.), *Biogeochemistry* (pp. 317–424). Elsevier-Perгамon.

- Michaelides, R. J., Schaefer, K., Zebker, H. A., Parsekian, A., Liu, L., Chen, J., et al. (2019). Inference of the impact of wildfire on permafrost and active layer thickness in a discontinuous permafrost region using the remotely sensed active layer thickness (ReSALT) algorithm. *Environmental Research Letters*, *14*, 035007. <https://doi.org/10.1088/1748-9326/aaf932>
- Miller, S. M., Miller, C. E., Commancie, R., Chang, R. Y.-W., Dinardo, S. J., Henderson, J. M., et al. (2016). A multiyear estimate of methane fluxes in Alaska from CARVE atmospheric observations. *Global Biogeochemical Cycles*, *30*, 1441–1453. <https://doi.org/10.1002/2016gb005419>
- Minsley, B. J., Pastick, N. J., Wylie, B. K., Brown, D. R. N., & Kass, M. A. (2016). Evidence for nonuniform permafrost degradation after fire in boreal landscapes. *Journal of Geophysical Research: Earth Surface*, *121*, 320–335. <https://doi.org/10.1002/2015jg003781>
- Muster, S., Riley, W. J., Roth, K., Langer, M., Cresto Aleina, F., Koven, C. D., et al. (2019). Size distributions of Arctic waterbodies reveal consistent relations in their statistical moments in space and time. *Frontiers of Earth Science*, *7*. <https://doi.org/10.3389/feart.2019.00005>
- Newman, B. D., Throckmorton, H. M., Graham, D. E., Gu, B., Hubbard, S. S., Liang, L., et al. (2015). Microtopographic and depth controls on active layer chemistry in Arctic polygonal ground. *Geophysical Research Letters*, *42*, 1808–1817. <https://doi.org/10.1002/2014gl062804>
- Olefeldt, D., & Roulet, N. T. (2012). Effects of permafrost and hydrology on the composition and transport of dissolved organic carbon in a subarctic peatland complex. *Journal of Geophysical Research*, *117*, G01005. <https://doi.org/10.1029/2011jg001819>
- Payn, R. A., Helton, A. M., Poole, G. C., Izurieta, C., Burgin, A. J., & Bernhardt, E. S. (2014). A generalized mechanistic model for applying thermodynamic, kinetic, and stoichiometric ecological theory to the biogeochemistry of aquatic microbial ecosystems. *Ecological Modelling*, *294*, 1–18. <https://doi.org/10.1016/j.ecolmodel.2014.09.003>
- Petrone, K. C., Hinzman, L. D., Shibata, H., Jones, J. B., & Boone, R. D. (2007). The influence of fire and permafrost on sub-arctic stream chemistry during storms. *Hydrological Processes*, *21*, 423–434. <https://doi.org/10.1002/hyp.6247>
- Porter, C., Morin, P., Howat, I., Noh, M.-J., Bates, B., Peterman, K., et al. (2018). *ArcticDEM*. Harvard Dataverse.
- Raymond, P. A., Hartmann, J., Lauerwald, R., Sobek, S., McDonald, C., Hoover, M., et al. (2013). Global carbon dioxide emissions from inland waters. *Nature*, *503*, 355–359. <https://doi.org/10.1038/nature12760>
- Regnier, P., Friedlingstein, P., Ciais, P., Mackenzie, F. T., Gruber, N., Janssens, I. A., et al. (2013). Anthropogenic perturbation of the carbon fluxes from land to ocean. *Nature Geoscience*, *6*, 597–607. <https://doi.org/10.1038/ngeo1830>
- Rinne, J., Tuittila, E.-S., Peltola, O., Li, X., Raivonen, M., Alekseychik, P., et al. (2018). Temporal variation of ecosystem scale methane emission from a boreal fen in relation to temperature, water table position, and carbon dioxide fluxes. *Global Biogeochemical Cycles*, *32*(7), 1087–1106. <https://doi.org/10.1029/2017gb005747>
- Rosentreter, J. A., Borges, A. V., Deemer, B. R., Holgerson, M. A., Liu, S., Song, C., et al. (2021). Half of global methane emissions come from highly variable aquatic ecosystem sources. *Nature Geoscience*, *14*, 225–230. <https://doi.org/10.1038/s41561-021-00715-2>
- Schuur, E. A. G., Bockheim, J., Canadell, J. G., Euskirchen, E., Field, C. B., Goryachkin, S. V., et al. (2008). Vulnerability of permafrost carbon to climate change: Implications for the global carbon cycle. *BioScience*, *58*, 701–714. <https://doi.org/10.1641/b580807>
- Schuur, E. A. G., McGuire, A. D., Grosse, G., Harden, J. W., Hayes, D. J., Hugelius, G., et al. (2015). Climate change and the permafrost carbon feedback. *Nature*, *520*, 171–179. <https://doi.org/10.1038/nature14338>
- Segers, R. (1998). Methane production and methane consumption: A review of processes underlying wetland methane fluxes. *Biogeochemistry*, *41*, 23–51. <https://doi.org/10.1023/a:1005929032764>
- Stackpole, S. M., Butman, D. E., Clow, D. W., Verdin, K. L., Gaglioti, B. V., Genet, H., & Striegl, R. G. (2017). Inland waters and their role in the carbon cycle of Alaska. *Ecological Applications*, *27*, 1403–1420. <https://doi.org/10.1002/eap.1552>
- Thornton, B. F., Wik, M., & Crill, P. M. (2016). Double-counting challenges the accuracy of high-latitude methane inventories. *Geophysical Research Letters*, *43*(12), 12569–12577. <https://doi.org/10.1002/2016gl071772>
- Throckmorton, H. M., Heikoop, J. M., Newman, B. D., Altmann, G. L., Conrad, M. S., Muss, J. D., et al. (2015). Pathways and transformations of dissolved methane and dissolved inorganic carbon in Arctic tundra watersheds: Evidence from analysis of stable isotopes. *Global Biogeochemical Cycles*, *29*, 1893–1910. <https://doi.org/10.1002/2014gb005044>
- Toming, K., Kotta, J., Uuemaa, E., Sobek, S., Kutser, T., & Tranvik, L. J. (2020). Predicting lake dissolved organic carbon at a global scale. *Scientific Reports*, *10*, 8471. <https://doi.org/10.1038/s41598-020-65010-3>
- Torn, M. S., & Chapin, F. S. (1993). Environmental and biotic controls over methane flux from Arctic tundra. *Chemosphere*, *26*, 357–368. [https://doi.org/10.1016/0045-6535\(93\)90431-4](https://doi.org/10.1016/0045-6535(93)90431-4)
- Townsend-Small, A., Åkerström, F., Arp, C. D., & Hinkel, K. M. (2017). Spatial and temporal variation in methane concentrations, fluxes, and sources in lakes in Arctic Alaska. *Journal of Geophysical Research: Biogeosciences*, *122*, 2966–2981. <https://doi.org/10.1002/2017JG004002>
- Tranvik, L. J., Downing, J. A., Cotner, J. B., Loiselle, S. A., Striegl, R. G., Ballatore, T. J., et al. (2009). Lakes and reservoirs as regulators of carbon cycling and climate. *Limnology & Oceanography*, *54*, 2298–2314. [https://doi.org/10.4319/lo.2009.54.6\\_part\\_2.2298](https://doi.org/10.4319/lo.2009.54.6_part_2.2298)
- Turetsky, M. R., Treat, C. C., Waldrop, M. P., Waddington, J. M., Harden, J. W., & McGuire, A. D. (2008). Short-term response of methane fluxes and methanogen activity to water table and soil warming manipulations in an Alaskan peatland. *Journal of Geophysical Research*, *113*, G00A10. <https://doi.org/10.1029/2007jg000496>
- Ueyama, M., Yazaki, T., Hirano, T., Futakuchi, Y., & Okamura, M. (2020). Environmental controls on methane fluxes in a cool temperate bog. *Agricultural and Forest Meteorology*, *281*, 107852. <https://doi.org/10.1016/j.agrformet.2019.107852>
- Veraart, A. J., Steenbergh, A. K., Ho, A., Kim, S. Y., & Bodelier, P. L. E. (2015). Beyond nitrogen: The importance of phosphorus for CH<sub>4</sub> oxidation in soils and sediments. *Geoderma*, *259–260*, 337–346. <https://doi.org/10.1016/j.geoderma.2015.03.025>
- Virkkala, A.-M., Aalto, J., Rogers, B. M., Tagesson, T., Treat, C. C., Natali, S. M., et al. (2021). Statistical upscaling of ecosystem CO<sub>2</sub> fluxes across the terrestrial tundra and boreal domain: Regional patterns and uncertainties. *Global Change Biology*, *27*, 4040–4059. <https://doi.org/10.1111/gcb.15659>
- Vonk, J. E., Tank, S. E., Bowden, W. B., Laurion, I., Vincent, W. F., Alekseychik, P., et al. (2015). Reviews and syntheses: Effects of permafrost thaw on Arctic aquatic ecosystems. *Biogeosciences*, *12*, 7129–7167. <https://doi.org/10.5194/bg-12-7129-2015>
- Walvoord, M. A., & Kurylyk, B. L. (2016). Hydrologic impacts of thawing permafrost—A review. *Vadose Zone Journal*, *15*, 6. <https://doi.org/10.2136/vzj2016.01.0010>
- Warwick, N. J., Cain, M. L., Fisher, R., France, J. L., Lowry, D., Michel, S. E., et al. (2016). Using  $\delta^{13}\text{C}\text{-CH}_4$  and  $\delta\text{D}\text{-CH}_4$  to constrain Arctic methane emissions. *Atmospheric Chemistry and Physics*, *16*, 14891–14908. <https://doi.org/10.5194/acp-16-14891-2016>
- Watts, J., Natali, S. M., Minions, C., Risk, D., Arndt, K. A., Zona, D., et al. (2021). Soil respiration strongly offsets carbon uptake in Alaska and Northwest Canada. *Environmental Research Letters*, *16*(8), 084051. <https://doi.org/10.1088/1748-9326/ac1222>
- Wessel, P., Luis, J. F., Uieda, L., Scharroo, R., Wobbe, F., Smith, W. H. F., & Tian, D. (2019). The generic mapping tools version 6. *Geochemistry, Geophysics, Geosystems*, *20*, 5556–5564. <https://doi.org/10.1029/2019gc008515>
- Yvon-Durocher, G., Allen, A. P., Bastviken, D., Conrad, R., Gudas, C., St-Pierre, A., et al. (2014). Methane fluxes show consistent temperature dependence across microbial to ecosystem scales. *Nature*, *507*, 488–491. <https://doi.org/10.1038/nature13164>

- Zarnetske, J. P., Haggerty, R., Wondzell, S. M., & Baker, M. a. (2011). Dynamics of nitrate production and removal as a function of residence time in the hyporheic zone. *Journal of Geophysical Research*, *116*, G01025. <https://doi.org/10.1029/2010jg001356>
- Zhang, H., Tuittila, E.-S., Korrensalo, A., Räsänen, A., Virtanen, T., Aurela, M., et al. (2020). Water flow controls the spatial variability of methane emissions in a northern valley fen ecosystem. *Biogeosciences Discussions*, 1–32. <https://doi.org/10.5194/bg-17-6247-2020>
- Zheng, J., RoyChowdhury, T., Yang, Z., Gu, B., Wulschleger, S. D., & Graham, D. E. (2018). Impacts of temperature and soil characteristics on methane production and oxidation in Arctic tundra. *Biogeosciences*, *15*, 6621–6635. <https://doi.org/10.5194/bg-15-6621-2018>